JOURNAL OF MATERIALS SCIENCE 28 (1993) 5809–5813

Dielectric relaxations in $SrTiO_3$ doped with La_2O_3 and MnO_2 at low temperatures

E. IGUCHI, K. J. LEE
Department of Mechanical Engineering and Materials Science, Faculty of Engineering, Yokohama National University, Tokiwadai, Hodogaya-Ku, Yokohama 240, Japan

In addition to the dielectric relaxation around 170 K in the cubic structure of $Sr_{1-3x/2}La_xTiO_3$, a similar relaxation was observed at about 70 K in the tetragonal structure with an activation energy in the range 0.13–0.16 eV which increases as x in $Sr_{1-3x/2}La_xTiO_3$ varies from 0.60–3.00 at %. This relaxation is explained by Skanavi's model and is discussed in terms of thermal motions of Ti^{4+} between potential minima produced by lattice distortions in the tetragonal structure. In order to provide a direct evidence for the suggestion that the dielectric relaxation around 170 K in the cubic is due to thermal motions of Ti^{4+}, dielectric properties on manganese-doped specimens, $Sr_{1-3x/2}La_xMn_yTi_{1-y}O_3$ with $x = 1.40 \times 10^{-2}$ and $y = 0.1 \times 10^{-2}$, were investigated because Mn^{4+} substitutes for Ti^{4+}. As well as the relaxation due to Ti^{4+}, this specimen exhibits another peak due to Mn^{4+} with an activation energy somewhat smaller than that of Ti^{4+}. The activation energies and the relative intensity of these relaxation processes are explained by the difference in ionic radii of Mn^{4+} and Ti^{4+} and the difference in formation energies of a strontium vacancy adjacent to Mn^{4+} and that to Ti^{4+}, which were calculated theoretically using a shell model.

1. Introduction

$SrTiO_3$ has a cubic perovskite structure at room temperature, but there is a phase-transition point from the cubic structure to tetragonal at 110 K [1–3]. According to Sakudo and Unoki [4], a further phase transition occurs from tetragonal to orthorhombic at 65 K.

After Skanavi and Matveeva [5] observed a dielectric dispersion associated with a relaxation around 170 K in n-type $SrTiO_3$ doped with Bi_2O_3, i.e. $Sr_{1-3x/2}Bi_xTiO_3$, the details of this relaxation in $Sr_{1-3x/2}M_xTiO_3$ were investigated [6, 7], where M represents rare-earth ions with a valence of + 3 such as La^{3+} which is the subject of this report. It is understood from the formula of $Sr_{1-3x/2}La_xTiO_3$, that two doped cations are substituted for two individual Sr^{2+} ions with the formation of one strontium vacancy (V_{sr}) [8]. It is generally accepted that the lattice distortions introduced by La^{3+} ions and associated vacancies are sufficient to produce more than one off-centre equilibrium position for the Ti^{4+} ion, and that the observed relaxation is associated with thermally activated motion between these equivalent minima, consequently increasing the dielectric constant [6–8]. Confirmatory evidence is, however, indispensable. If some impurity ion is substituted for Ti^{4+} in $Sr_{1-3x/2}La_xTiO_3$, one can expect another dielectric relaxation peak due to these impurities at the titanium sites. A relaxation such as this, if observed experimentally, must support the analysis described above. Mn^{4+} is one candidate of such an impurity ion because this ion is confirmed experimentally by electron spin resonance (ESR) to substitute for Ti^{4+} in $SrTiO_3$, but the amount of Mn^{4+} ions doped was very small [9].

On the other hand, it is also of great significance to investigate dielectric properties in the tetragonal $Sr_{1-3x/2}La_xTiO_3$ below 110 K, but, unfortunately, there are no reports in the literature of dielectric behaviour at lower temperatures. From this point of view, we have carried out dielectric measurements of these oxides at temperatures below the transition point from the cubic to tetragonal structure.

This report presents the dielectric properties at temperatures below 110 K and the investigation of manganese-doped effects on the dielectric dispersion around 170 K in $Sr_{1-3x/2}La_xTiO_3$.

2. Experimental procedure

$Sr_{1-3x/2}La_xTiO_3$ ceramics were prepared by the conventional solid-state technique [10], where $x = 0.60$–3.00 at %. The specimen is numbered using terminology such as L-1.00, where the number (e.g. 1.00) denotes the amount (at %) of La_2O_3. We also prepared samples of $Sr_{1-3x/2}La_xTi_{1-y}Mn_yO_3$ for the reason as described in Section 1. Powders of $SrCO_3$, La_2O_3, MnO_2 (Johnson Matthey, 99.999% pure) and TiO_2 (Aldrich Chemical, 99.99% pure) were used. After the final sintering at 1723 K, the specimens were cooled to room temperature in the furnace very slowly at a rate less than 50 K h^{-1}. Powder X-ray measurements indicated no phases other than $SrTiO_3$ at room temperature, being independent of the amount of

0022–2461

La_2O_3 or MnO_2. Flat surfaces of specimens were coated with an In–Ga alloy in 7:3 ratio by a rubbing technique to produce the electrode, which gives a good ohmic contact. HP 4274A and 4275A LCR meters were used for measurement of capacitances. The applied frequencies employed were in the range 100 Hz–2 MHz. A copper–constantan thermocouple precalibrated at 4.2, 77 and 273 K, was used for the temperature measurements.

3. Results and discussion

3.1. Dielectric properties in $Sr_{1-3x/2}La_xTiO_3$ below 110 K

Fig. 1 shows the typical results of the specimen L-1.4 on the frequency dependencies of dielectric properties (ε' and $\tan\delta$) as a function of temperature. A dielectric dispersion and a dielectric relaxation peak show around 70 K in the dielectric constant and $\tan\delta$, respectively. Arrhenius relations of applied frequencies and $1/T_m$ produced good straight lines, where T_m denotes the peak temperature of $\tan\delta$. The activation energy obtained in these plots increases from 0.13–0.16 eV with the amount of La_2O_3 increasing, where that of L-1.4 is 0.14 eV. These features obtained in the tetragonal structure (i.e. dielectric dispersions and the increase in the activation energy with increasing amount of La_2O_3) are quite similar to those observed in the cubic structure around 170 K [5–8]. In view of these similarities, the relaxation is likely to be of the type discussed, in that in the cubic structure, lattice-distortions are also introduced in the tetragonal structure by La^{3+} and V_{Sr}, and a thermally activated motion of Ti^{4+} ions between potential minima takes place at temperatures below 110 K. The theoretical analysis proposed by Skanavi *et al.* [8] also confirms this possibility. The activation energy, U, for this thermal motion has the form

$$U = \frac{k_B T_2^* T_2^{**}}{T_2^{**} - T_2^*} \ln\left[\frac{\omega^{**} T_2^* D^{*2}}{\omega^* T_2^{**} D^{**2}} \left(\frac{\varepsilon_0^*}{\varepsilon_0^{**}}\right)^{1/2}\right] \quad (1)$$

where $D = (\varepsilon'_{max} - \varepsilon_\infty)/\varepsilon''$, T_1 and T_2 are the temperatures of maximum ε' and of maximum $\tan\delta$, $\varepsilon'' = \varepsilon'_{max} \tan\delta$ at T_1, ε_0 and ε_∞ are the static dielectric constant and the constant at high frequencies at T_2, and the symbols * and ** refer to frequencies ω^* and ω^{**}.

Because this analysis requires values for ε_0 and ε_∞, these were determined using Cole–Cole plots. Fig. 2 shows the Cole–Cole plots at 68 and 80 K which are T_2 at $\omega = 2\pi \times 1$ kHz and $2\pi \times 40$ kHz, respectively for the specimen L-1.4. The values determined by least-squares methods are given in Table I along with other parameters. The activation energy is then estimated to be 0.15 eV, which agrees with the value determined from the Arrhenius plots, i.e. 0.14 eV.

Fig. 1 exhibits another very small relaxation in $\tan\delta$ around 30 K and the temperature dependencies of the dielectric constant deviate from the Curie–Weiss law in the temperature range where the relaxation appears. Arrhenius plots of applied frequencies versus $1/T_m$ produce straight lines with an activation energy of $\sim$0.07 eV. At the moment, the mechanism for this relaxation is unknown. Referring to the phase transition from the tetragonal structure to orthorhombic at 65 K [4], there must be a correlation between this relaxation and the orthorhombic structure.

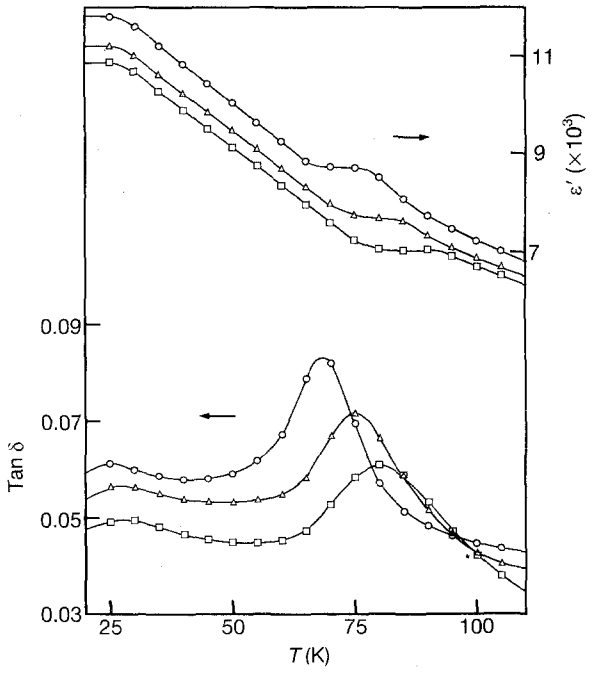

Figure 1 Dielectric constants, ε', and dielectric loss tangents, $\tan\delta$, of the specimen L-1.4 in the temperature range of 20–110 K with applied frequencies, f: (○) 1 kHz, (△) 10 kHz, and (□) 40 kHz.

3.2. Manganese-doped effect on dielectric properties above 110 K

3.2.1. Splitting of the dielectric relaxation peak

As described in Section 1, the dielectric dispersion associated with a relaxation around 170 K was investigated in detail. The dielectric measurements on our $Sr_{1-3x/2}La_xTiO_3$ specimens exhibit the same results as reported previously [5–8] and the activation energy in the Arrhenius relation of applied frequencies versus $1/T_m$ increases from 0.22 eV to 0.29 eV as x increases from 0.6×10^{-2} to 3×10^{-2}. Fig. 3 demonstrates the typical results on frequency dependencies of the sample L-1.40, i.e. nominally $Sr_{0.979}La_{0.014}TiO_3$, as a function of temperature. The activation energy obtained in the Arrhenius relation is 0.25 eV. Although the ionic model proposed by Skanavi *et al.* is very successful in the analyses on these dispersions in the cubic structure [6–8], some direct evidence is required. To this end, we prepared samples of $Sr_{1-3x/2}La_xTi_{1-y}Mn_yO_3$, where $x = 1.40\times10^{-2}$ (1.40 at %) and $y \simeq 0.1\times10^{-2}$ ($\simeq$0.1 at %). Because the lattice distortions induce the dielectric relaxation due to thermal motions of Ti^{4+} ions, one can expect a similar relaxation due to Mn^{4+} ions incorporated at titanium sites with an activation energy somewhat different from that of Ti^{4+}.

Fig. 4 demonstrates the results for the sample doped with 0.1 at % MnO_2, i.e. $y = 0.1\times10^{-2}$. For $\tan\delta$, the vertical axis in this figure plots the realistic values obtained by extracting background values from ex-

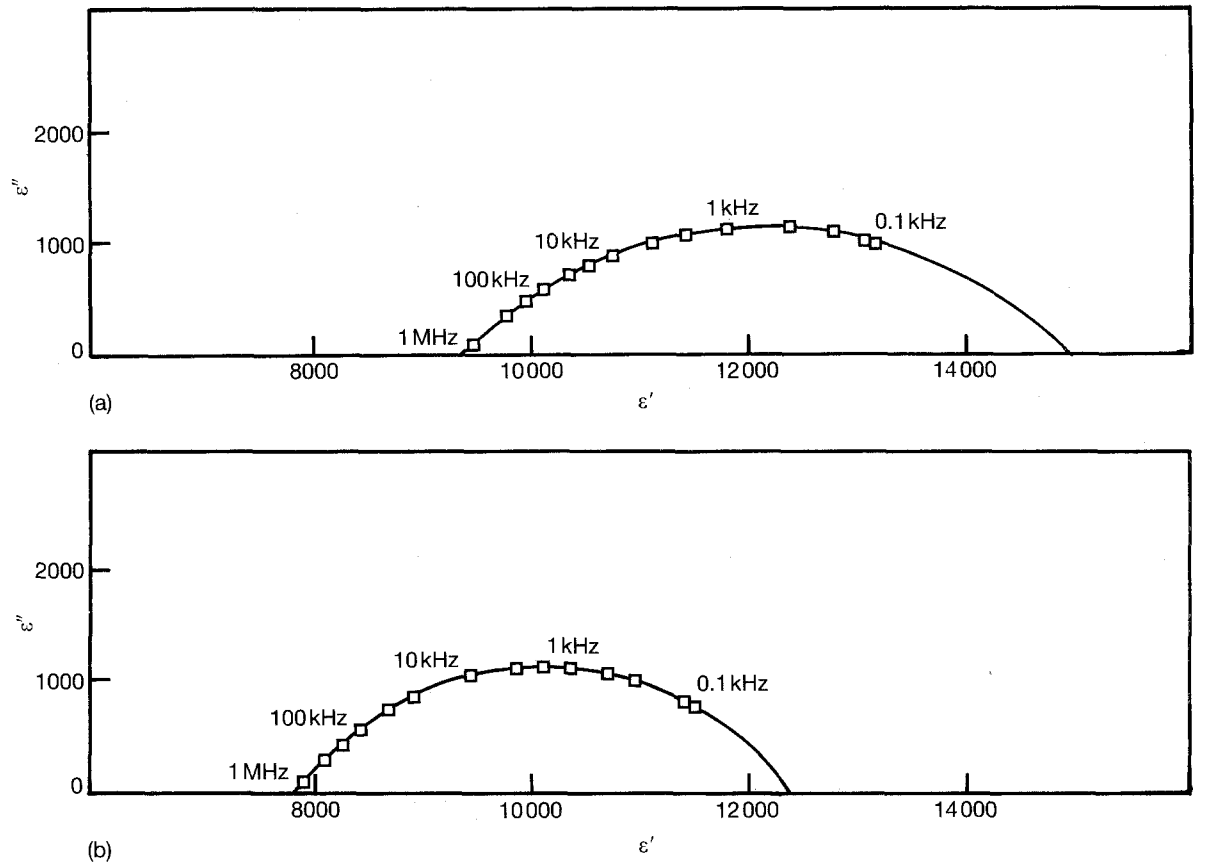

Figure 2 Cole–Cole plots of the specimen L-1.4 at T_2 = (a) 68 and (b) 80 K.

TABLE I The parameters used in the analyses of Skanavis *et al.* for the specimen L-1.4, T_1 and T_2 are the temperature of maximum ε′ and that of maximum tan δ, $\varepsilon'' = \varepsilon'_{max} \tan\delta$ at T_1, and ε_0 and ε_∞ are the static dielectric constant and the constant at high frequencies at T_2

f (kHz)	T_1 (K)	T_2 (K)	ε'_{max}	ε''	ε_0	ε_∞	U (eV)
1	78	68	10383.8	761.9	14900	9400	0.15
40	92	80	8535.8	587.3	12400	7820	

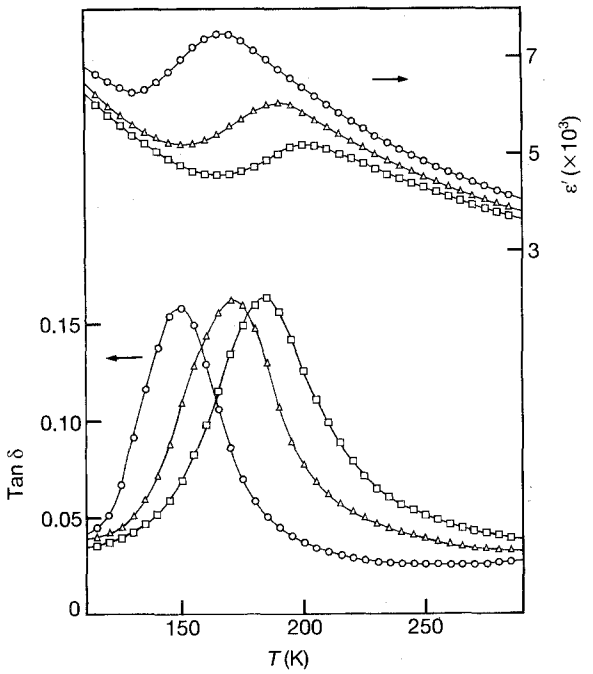

Figure 3 Dielectric constants, ε′, and dielectric loss tangents, tan δ, of the specimen L-1.4 in the temperature range 110–290 K with applied frequencies, f: (○) 1 kHz, (△) 10 kHz, and (□) 40 kHz.

perimental data. The relaxation peak becomes distorted more remarkably as the applied frequency increases, that is, it consists of two individual peaks. Fig. 4 includes two theoretical curves calculated using the Debye equation, where we have employed the activation energy of 0.25 eV obtained in sample L-1.40 for one relaxation peak which corresponds to the energy required for the thermal motion of Ti^{4+}, while the activation energy of the second peak and the relative intensity of the loss tangent at maximum, $(\tan\delta)_{max}$, between two peaks is determined by adjusting them to fit the experimental data. Then, the second peak has an activation energy of 0.23 eV, which must represent the activation energy for the thermal motion of Mn^{4+} The resultant profile of these two peaks is in good agreement with the experimental data within reasonable error. The energy required for the thermal motion of Mn^{4+} is somewhat smaller than that of Ti^{4+}. This must be closely related to the difference between ionic radii, 0.054 nm (Mn^{4+}) and 0.060 nm (Ti^{4+}) [11]. The ionic radius of Mn^{4+}, being smaller than that of Ti^{4+}, must enhance thermal motions of Mn^{4+} more frequently with an activation energy smaller than that of Ti^{4+}. In order to examine

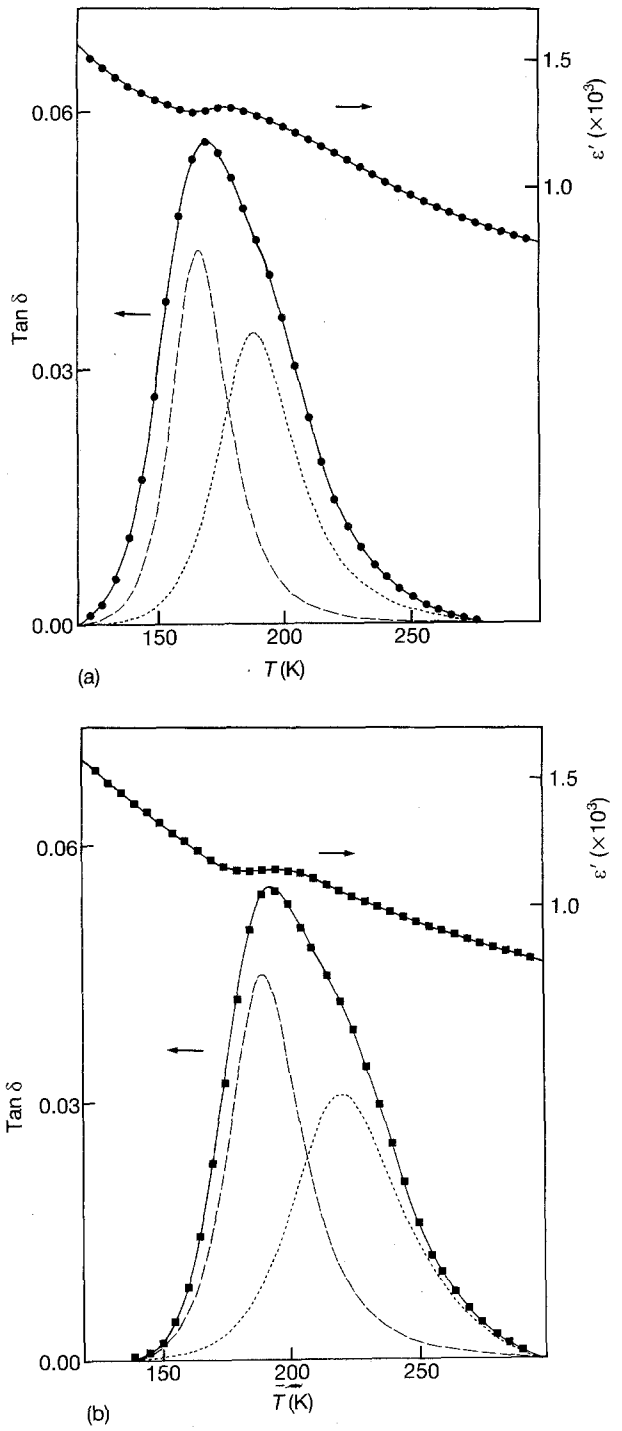

Figure 4 Dielectric constants, ε', and dielectric loss tangents, tan δ, of the specimen $Sr_{1-3x/2}La_xTi_{1-y}Mn_yO_3$ with $x = 1.40 \times 10^{-2}$ (1.40 at %) and $y = 0.1 \times 10^{-2}$ (0.1 at %), (a) $f = 20$ kHz and (b) $f = 200$ kHz. The realistic tan δ values obtained by extracting background values from experimental data are plotted. The loss tangent curves repesent the theoretical ones calculated by the Debye equation with activation energies of (– – –) 0.25 eV and (· · ·) 0.23 eV, respectively.

the reproducibility of the peak splitting, we prepared a sample with $y = 0.12 \times 10^{-2}$ (0.12 at %). The distortion of the peak was again recognized.

3.2.2. Relative intensity between split peaks

According to the Debye theory, the maximum value of tan δ is proportional to the concentration of thermally activated ions. As shown in Fig. 4, the ratio of the intensity of the dielectric peak due to Ti^{4+} to that of

TABLE II The parameters employed in calculations of vacancies. The repulsive energy between ions i and j, is represented by a Born–Mayer potential, i.e. $(E_R)_{ij} = A_{ij} \exp(-B_{ij} r_{ij})$, where A and B are Born–Mayer constants and r is the ionic spacing. The van der Waals interaction energy between ions i and j, has the form $(E_W)_{ij} = C_{ij}/r_{ij}^6$.

(a)

Ion pair	Born–Mayer constant		van der Waals constant,
	A (eV)	B (nm^{-1})	C (10^{-6} eV nm^{-6})
Ti^{4+}–Ti^{4+}	7.090×10^5	80.21	19.43
Sr^{2+}–Sr^{2+}	8.379×10^3	39.93	96.85
Ti^{4+}–Sr^{2+}	1.166×10^4	46.40	42.03
O^{2-}–O^{2-}	4.388×10^2	32.30	23.78
Ti^{4+}–O^{2-}	1.902×10^3	31.75	12.88
Sr^{2+}–O^{2-}	1.841×10^3	30.77	34.74
Ti^{4+}–Mn^{4+}	9.065×10^4	68.49	70.19
Sr^{2+}–Mn^{4+}	1.782×10^4	48.67	15.09
Mn^{4+}–O^{2-}	2.049×10^3	31.97	45.61

(b)

	Sr^{2+}	Ti^{4+}	O^{2-}	Mn^{4+}
Electronic polarizability in free state (10^{-3} nm^3)	0.860	0.186	3.88	0.188
Electronic polarizability in lattice (10^{-3} nm^3)	1.721	0.599	1.991	0.211
Ionic polarizability (10^{-3} nm^3)	0.0	0.382	1.802	
Shell parameter	6.687	7.455	1.642	4.654

(c)

Lattice constant (nm)	0.390 51
Static dielectric constant	310
Dielectric constant at high frequencies	5.20

Mn^{4+} is about 1.5, in spite of the fact that the ratio of the amount of Ti^{4+} ions to that of Mn^{4+} is 999. In order to examine this problem, we have calculated formation energies of strontium vacancies adjacent to Mn^{4+} or Ti^{4+} using a polarizable point-ion shell model which we have often employed in energy calculations of oxides [12–16]. We followed fully the method of our calculations in n-type $BaTiO_3$ which is isomorphous with $SrTiO_3$ [16]. Table II gives the parameters used in the calculations. (An appendix which explains how to determine these parameters will be furnished by the authors upon request.)

The shell model is based upon calculations of dipole moments induced by the electric field due to the effective charge of an imperfection such as a vacancy. In the case of V_{Sr}, the effective charge is $-2e$. The dipole moments in a spherical region of diameter $3.32a$ around V_{Sr} have been determined by the matrix technique, where a is the lattice constant. Dipole moments in the shell of diameter $12.12a$ outside the spherical region have been evaluated by the approximate method of Mott and Littleton [17]. Every ion in the remainder of the crystal is fixed (see [16]).

Table III summarizes Madelung, E_M, repulsive, E_R, and van der Waals energies, E_W, of O^{2-}, Sr^{2+} adjacent to Ti^{4+} and that to Mn^{4+} with the energies required to form vacancies of these ions in the rigid, unpolarized lattice, $(E_F)_0$. The formation energy of a

TABLE III Madelung, E_M, repulsive, E_R, and van der Waals, E_W, energies of Sr^{2+} adjacent to Ti^{4+} and those of Sr^{2+} adjacent to Mn^{4+} with the results for O^{2-}. $(E_F)_0$ denotes formation energies of vacancies of these ions in a rigid, unpolarized lattice

Ion	E_M (eV)	E_R (eV)	E_W (eV)	$(E_F)_0$ (eV)
Sr^{2+} adjacent to Ti^{4+}	− 39.73	4.55	− 1.52	18.35
Sr^{2+} adjacent to Mn^{4+}	− 39.73	4.55	− 1.51	18.34
O^{2-}	− 47.61	9.72	− 1.37	19.63

TABLE IV Lattice-relaxation energies and formation energies, E_F, of strontium vacancies adjacent to Ti^{4+} or Mn^{4+} and oxygen vacancies, where the relaxation energy consists of the changes in Madelung, repulsive and van der Waals energies, i.e., ΔE_M, ΔE_R and ΔE_W, and the polarization energy, E_P

Ion	ΔE_M (eV)	ΔE_R (eV)	ΔE_W (eV)	E_P (eV)	E_F (eV)
Sr^{2+} adjacent to Ti^{4+}	6.91	− 3.29	− 0.89	− 8.57	12.51
Sr^{2+} adjacent to Mn^{4+}	7.00	− 3.39	− 1.03	− 8.57	12.35
O^{2-}	− 6.83	4.13	− 1.03	− 10.15	5.75

vacancy, E_F, is the sum of $(E_F)_0$ and the lattice-relaxation energy which consists of the changes in Madelung, repulsive and van der Waals energies, i.e. ΔE_M, ΔE_R and ΔE_W, and the polarization energy, E_P [12–16]. Lattice-relaxation and formation energies of these vacancies are shown in Table IV. The formation energy of a doubly charged oxygen vacancy was calculated because the experimental result on this point defect [18], 5.76 eV, was used as a criterion in the determination of shell parameters of ions (see [16]). As described before, the specimens were cooled to room temperature very slowly after the final sintering. Then, the ratio of the amount of V_{Sr} adjacent to Ti^{4+} to that of V_{Sr} adjacent to Mn^{4+} at room temperature is

$$\begin{aligned} &999 \exp(-12.51/300k_B)/\exp(-12.35/300k_B) \\ &= 999 \exp(-0.16/300k_B) \\ &\simeq 2 \end{aligned} \quad (2)$$

where k_B is the Boltzmann's constant. This ratio is in good agreement with the experimental result, i.e. ~ 1.5, despite omitting a coupling constant representing the Jahn–Teller distortions of manganese ions. A more precise calculation, as in our previous report on a polaron in $BaTiO_3$ [16], would be possible if we could take into account the coupling constant. Unfortunately, no experimental values relevant to such distortions in these materials are available.

Speculation such as this indicates conclusively that the result in Fig. 4 is direct evidence for the thermally activated motions of titanium ions between off-centre equilibrium positions. However, manganese-doped effects cannot be recognized clearly on the dielectric properties around 70 K. This must be mainly due to the low intensity of this relaxation peak.

Fig. 4 also demonstrates temperature dependencies of dielectric constants, ε'. These curves contain dielectric dispersions, but not so remarkably compared with the result of the specimen L-1.4 (see Fig. 3) and values of dielectric constants reduce nearly to those of pure $SrTiO_3$. The result in Fig. 4 suggests a high possibility that Jahn–Teller distortions of manganese ions offset the lattice distortions introduced by La^{3+} and V_{Sr} and, consequently, decrease the number of off-centre equilibrium positions for thermal motions of Ti^{4+} or Mn^{4+}. In fact, the maximum value of $\tan\delta$ in L-1.4 (see Fig. 3) reduces to nearly half, even when 0.1 at % MnO_2 is doped (see Fig. 4). Michel and Raveau [19] suggested that Jahn–Teller distortions are so profound that they change even a band structure in an oxide when the amount of dopants such as manganese ions exceeds some limited value.

Acknowledgements

This project was supported by a Grant-in-Aid for Science Research (3650573) from the Ministry of Education, Japan, and The Murata Science Foundation. The authors are grateful to A. Iguchi, E. Nakamura and K. Takeda for their assistance in this project.

References

1. H. UNOKI and T. SAKUDO, *J. Phys. Soc. Jpn* **23** (1967) 546.
2. P. A. FLEURY, J. F. SCOTT and J. M. WORLOCK, *Phys. Rev. Lett.* **21** (1968) 16.
3. G. SHIRANE and Y. YAMADA, *Phys. Rev.* **177** (1969) 858.
4. T. SAKUDO and H. UNOKI, *Phys. Rev. Lett.* **26** (1971) 26.
5. G. I. SKANAVI and E. N. MATVEEVA, *Sov. Phys. JET* **3** (1957) 905.
6. D. W. JOHNSON, L. E. CROSS and F. A. HUMMEL, *J. Appl. Phys.* **41** (1970) 2828.
7. T. Y. TIEN and L. E. CROSS, *Jpn. J. Appl. Phys.* **6** (1967) 459.
8. G. I. SKANAVI, I. M. KSENDZOV, V. A. TRIGUBENKO and V. G. PROKHVATILOV, *Sov. Phys. JET* **6** (1958) 250.
9. K. A. MÜLLER, *Phys. Rev. Lett.* **2** (1959) 341.
10. I. BURN and S. NEIRMAN, D. A. KLEIMMAN and L. E. HAWARTH, *Mater. Sci.* **17** (1982) 3510.
11. R. D. SHANNON and C. T. PREWITT, *Acta Crystallogr.* **18** (1968) 141.
12. H. SAWATARI, E. IGUCHI and R. J. D. TILLEY, *J. Phys. Chem. Solids* **43** (1982) 1147.
13. K. AIZAWA, E. IGUCHI and R. J. D. TILLEY, *Proc. R. Soc. Lond.* **A394** (1984) 299.
14. F. MATSUSHIMA and E. IGUCHI, *J. Phys. Chem. Solids* **47** (1986) 45.
15. E. IGUCHI, T. YAMAMOTO and R. J. D. TILLEY, *ibid.* **49** (1988) 205.
16. E. IGUCHI and A. TAMENORI, *Phys. Rev.* **B45** (1992) 697.
17. N. F. MOTT and M. J. LITTLETON, *Trans. Faraday Soc.* **34** (1938) 485.
18. H. YAMADA and G. R. MILLER, *J. Solid State Chem.* **6** (1973) 169.
19. C. MICHEL and B. RAVEAU, *Rev. Chim. Minéral.* **21** (1984) 407.

Received 19 June 1992
and accepted 20 April 1993